INDUCED ANNULAR WATER FILM EVAPORATOR FOR AIR TO REFRIGERANT HEAT EXCHANGE ENHANCEMENT IN A LITHIUM BROMIDE – WATER ABSORPTION REFRIGERATION SYSTEM

A. C. Bwalya, H. Sabir and M. Raine

Kingston University
Department of Mechanical, Aeronautical and Production Engineering
Friars Ave., London SW15 3DW, U.K.

ABSTRACT

A conceptual design of a tubular water evaporator for lithium bromide – water absorption refrigeration systems that circumvents the requirement for two heat exchangers by exchanging heat directly with the fluid to be cooled is described. The technique employed to enhance heat transfer entails a capillary induced thin 'annular' refrigerant film inside the evaporator tube. The pertinent heat transfer characteristics of the proposed evaporator design are demonstrated as part of an investigative programme having experimental and mathematical components.

The analytical results, obtained using existing single phase and two phase boiling heat transfer correlations from the literature, show that a heat transfer rates of up to 470 W and overall heat transfer coefficients of up to 55 W/m^2-K can be achieved for a unfinned evaporator with an external heat transfer area of 0.25m^2, giving a maximum heat flux of about 6 kW/m^2, for air velocities up to 4 m/s.

KEYWORDS

evaporator, lithium bromide – water, absorption refrigeration, heat transfer

1. INTRODUCTION

In the last decade, mounting environmental concerns, backed by overwhelming scientific evidence, about the ozone destroying behaviour and global warming potential of chlorofluorocarbons (CFCs) and hydrochlorofuorocarbons (HCFCs), which were the commonly used refrigerants prior to the 1990s, culminated in the phase out of CFCs in 1995 in EU countries. In addition, the Kyoto Protocol of 1997 has cast doubt on the long-term availability of new Hydrofluorocarbons (HFCs) based refrigerants, which despite being ozone-friendly are potent global warmers. International opinion is unanimous that the natural fluids air, water, carbon dioxide, hydrocarbons and ammonia are the way forward. This scenario has prompted a renewed interest in alternative refrigeration systems employing environmentally benign working fluids such as the Lithium Bromide – Water (LiBr-H_2O) absorption refrigeration system, which is the subject of this paper, where water is the refrigerant. Being heat driven, absorption refrigeration systems are particularly attractive in situations where cooling is required for, say process control and air-conditioning, when excess thermal energy is available.

In LiBr-H_2O absorption systems, hydrostatic head effects due to the low operating pressure (e.g., 8.7 kPa at a saturation temperature of 5 ^{O}C for water) in the evaporator preclude the use of pool boiling type flooded evaporators in which the fluid to be cooled would exchange heat directly with the refrigerant (water). In practice, a 'falling-film' heat exchanger is employed and the refrigerant is sprayed on to a bank of tubes through which a secondary refrigerant flows. The secondary refrigerant subsequently cools the air in a second heat exchanger (for air-conditioning applications), with additional complexity and decreased thermal efficiency as obvious penalties.

This work aims to circumvent the requirement for two heat exchangers by using an evaporator, which exchanges heat directly with the air to be cooled. This can be achieved by increasing the heat transfer area (wetted area) inside of the tube, where the refrigerant flows, without impeding the flow of the vapour generated. To this end, a wetting technique that entails a capillary induced thin 'annular' refrigerant film inside the evaporator tube is employed. Analytical results are presented to demonstrate the pertinent performance characteristics of the proposed evaporator design. Use is made of an existing single phase correlation and a two-phase boiling heat transfer correlation from the literature in a mathematical model to estimate the relevant heat transfer performance characteristics, such as refrigerating capacity and overall heat transfer coefficient.

The experimental work is underway and therefore the accuracy of the analytical results presented in this paper is unverified. In this light, the results are preliminary.

2. CAPILLARY WICK STRUCTURES

Many basic materials and surface forms are used in the construction of wick structures of which the most commonly used are: woven metal screens, metal felts and foams, sintered metal powders and circumferential and axial grooves which are machined into the inside wall of the pipe. Wick structures are used extensively in the field of heat pipes. A comprehensive treatment of heat pipe science and technology can be found in the widely available literature, for example [0].

A. C. Bwalya, alex@bwalya.freeserve.co.uk

Wick structures made from woven metal screens, metal felts and foams are inherently difficult to hold against the inside wall of tube. Eames et al. [1] and Sabir and Eames [3] used a glass fibre cloth wick, which was held against the inner tube wall by a stainless steel mesh and noted that there was poor thermal contact that increased thermal resistance between the wick and the tube wall. In addition, the requirement that the wick material withstands the high soldering temperatures encountered during fabrication of the evaporator resulted in the use of fibreglass, which has poor thermal properties. In this work only sintered metal powder wicks and grooved wicks are investigated, all of which are mechanically and thermally superior to woven wicks, metal felts and foam wicks.

Three circumferential groove geometries characterised by width of groove, W, width of land, L, and depth, B, are considered, namely: semi-circular, rectangular and triangular, as shown in Figure 1. The capillary height is a function of the hydraulic radius (hereinafter referred to as the effective radius, r_e), which is given by Equation (1) [1] and the contact angle, which governs wetting behaviour and consequently capillary height. In order to ensure that the entire inner surface area is completely wetted, each geometry must have a capillary height, given by Equation (2) [1], which is at least equal to the inner diameter (approximately 26 mm) of the evaporator tube. Due to the lack of published contact angle data for water on copper surfaces, a contact angle of zero, i.e. complete wetting, was assumed.

$$r_e = \frac{2 \times flow\ area}{wetted\ \ perimeter} \tag{1}$$

$$h = \frac{\frac{2\sigma}{r_e}\cos\theta}{\rho g} \tag{2}$$

The sintered metal powder wick is made by sintering a metal powder to the inner wall of the tube, resulting in intimate contact between the wick and the wall, and the between the individual spherical metal particles that make up the wick. Sintered metal powder wicks have larger capillary pumping pressures than groove wicks owing to their smaller effective capillary radii.

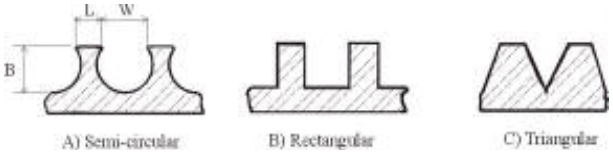

Figure 1: Cross-sections of the three open capillary grooves, characterised by; width of land – L, depth – B and width of groove – W.

2.1 Maximum Thermal Capacity

The maximum heat rate supported by each capillary structure is given by Equation (3), which is a form of the Hagen-Poiseulle [0] equation, with the driving pressure difference given by the difference between the maximum capillary head corresponding to the groove dimensions and the hydrostatic head imposed by the tube dimensions (i.e. inner diameter).

$$q_{max} = \frac{r_e^4 h_{fg}}{4\mu_l D_i}\left[\frac{\frac{2\sigma}{r_e}}{\rho g} - D_i \rho g\right] \tag{3}$$

Figure 2 shows the maximum theoretical heat rate that can be supported by each of the three groove structures. The groove depth was varied while the groove width and land are kept constant at 0.6 mm and 0.5 mm, respectively. The maximum heat rate supported by the triangular grooves is significantly lower than that for the semi-circular and rectangular grooves. This is because the triangular grooves have a smaller hydraulic radius and hence the greatest resistance to flow at comparable hydraulic radii. It is interesting to note that the semi-circular groove shows a distinct peak at a depth of between 0.5 and 0.6 mm. This is due to the combined effects of viscous resistance and capillary head. At smaller groove depths, viscous resistance diminishes the maximum heat rate despite the existence of a large capillary head. As the channel deepens, i.e. increasing hydraulic radii, reducing viscous resistance results in an overall increase in the maximum heat rate until a peak is reached when reducing capillary head due to the larger hydraulic head causes the heat rate to drop. This trend is shown by all the grooves.

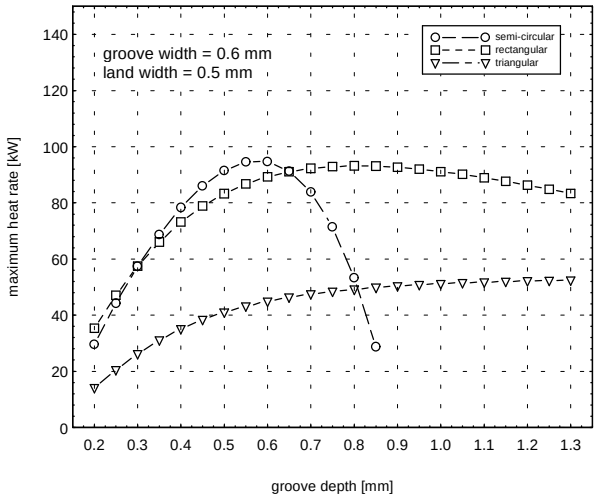

Figure 2: Maximum heat rate per metre length of grooved evaporator tube

3. ANALYSIS OF HEAT TRANSFER

Although heat transfer in boiling and condensation has been intensely investigated over the last three decades and many empirical heat transfer correlations exist, a literature review conducted by the authors revealed that there are currently no boiling heat transfer correlation that have been developed specifically for use at sub-atmospheric pressures in the order of 0.8 kPa. This is largely because the great majority of correlations found in the literature have been developed for

application in steam generating plant and related process plant where high operating pressures are the norm. The Roshenow pool boiling correlation [4] given by Equation (5), was the only correlation that was found to be applicable over a wide range of reduced pressures without any explicit restrictions. Two other boiling heat transfer correlations were considered, namely: Stephan and Abdelsalam [5] and Copper [6], both of which did not give meaningful results since they are only applicable in the reduced pressure (i.e. ratio of operating pressure to critical pressure) range 10^{-4} to 0.9; The reduced pressure of interest in this work is about 10^{-5}, which corresponds to a saturation temperature of about 5 ^{O}C (0.87 kPa) for water.

3.1 Physical Model

It is assumed that the liquid (water) completely wets the surface, i.e. zero contact angle, and that at entry to the evaporator, the refrigerant is in a saturated liquid state. It is also assumed that the liquid in the capillary passages is not flowing and boiling conditions can be approximated by pool boiling.

The evaporator is located in a wind tunnel, which has a square cross-section measuring 310 x 310 mm. The evaporator consists of a bank of nine tubes of O.D 28.6 mm ($1\frac{1}{8}''$ copper) and effective length 310 mm., in a staggered arrangement, with five tubes in the first row and four tubes in the second row, as illustrated in Figure 3.

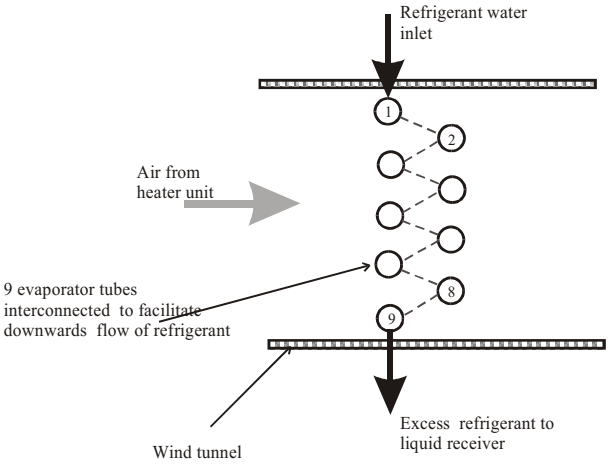

Figure 3: Layout of evaporator tubes

Given the velocity of air in the wind tunnel and its inlet temperature, the mean convective heat transfer coefficient outside the bank of tubes was computed using Zhukaushas' correlation [7], Equation (4)

$$Nu = 0.35\, S_{TL}\, \mathrm{Re}_{D_o,\max}^{0.6}\, \mathrm{Pr}^{0.36} \left(\frac{\mathrm{Pr}}{\mathrm{Pr}_s}\right)^{1/4} \quad \begin{bmatrix} 0.7 < \mathrm{Pr} < 500 \\ 1000 < \mathrm{Re}_{D_o,\max} < 2\times10^6 \end{bmatrix} \tag{4}$$

Where S_{TL} is the ratio of transverse pitch to lateral pitch of the tubes and all properties, except Pr_s are evaluated at the arithmetic mean of the fluid inlet and outlet temperatures.

3.1.1 Grooved Tubes

For the grooved tubes, Rohsenow's pool boiling heat transfer correlation, Equation (5) [7], was used to determine the heat flux on the boiling surface:

$$q'' = \mu_l h_{fg} \left[\frac{g\left(\rho_l - \rho_g\right)}{\sigma}\right]^{\frac{1}{2}} \left(\frac{Cp_l \Delta T_{sat}}{C_{sf} h_{fg}\, \mathrm{Pr}_l}\right)^3 \tag{5}$$

The coefficient C_{sf} depends on surface-liquid combinations and is best determined experimentally. This is one disadvantage of this correlation. For water-copper, C_{sf} values for scored and polished surfaces are 0.0068 and 0.0130 [7] respectively. Boiling inception superheats are greater for polished surfaces than they are for rough surfaces. However, the contact angle for a smooth surface is smaller (better wetting) than that for a rough surface. Hence a compromise must be struck between the two conflicting requirements of low boiling inception superheat (rough surface) and small contact angle (smooth surface) which is required for better wetting characteristics. A scored surface with a C_{sf} value of 0.0068 was assumed in this work.

3.1.2 Porous Wick

In the case of the porous wick, the expression derived by Madhusudana and Balakrishnan [8], Equation (6), which assumes a close packed arrangement of spherical metal powder particles of uniform diameter was used:

$$q'' = 2.4\times10^{-4} \frac{\rho_l \rho_g^2 K\, h_{fg}^2 \left(\delta/d\right)^{0.8} \Delta T_{sat}\, Ja^{0.22}}{\mu_g\, \delta\, T_{sat} \left(\rho_l - \rho_g\right) \varepsilon^{1.23}} \tag{6}$$

In both cases, the overall boiling heat transfer coefficient was taken to be the sum of the pool boiling term and single phase convective term (due to vapour velocity). This was done because the conditions in the evaporator are not completely static; the vapour generated flows through the tubes and hence, the convective effects, if significant, would have to be accounted for. However, calculations indicated that the single phase convective heat transfer coefficient was less than 2% of the pool boiling heat transfer coefficient, at the conditions considered. The heat transfer coefficient controls the boiling process and is dependent on the fluid properties, fluid flow rate, type of flow and channel geometry and surface conditions.

The pool boiling heat transfer coefficient, h_{pb}, is given by equation (7), where ΔT_{sat} is the temperature difference driving heat transfer, i.e. the difference between the wall temperature and the saturation temperature of refrigerant;

$$h_{pb} = \frac{q''}{\Delta T} \qquad (7)$$

The single phase convective heat transfer coefficient for the vapour alone was calculated using the Dittus-Boelter equation [7]. The result, i.e. combined single phase and boiling heat rate, was compared with the external heat rate calculated using the outside convective heat transfer coefficient at the same wall temperature. An iterative computation scheme, using a FORTRAN 77 computer program, was carried out, logically adjusting the wall temperature until a value was reached at which the external and internal heat rates are equal. The overall heat transfer coefficient, based on the outside area, was calculated using the inside and outside heat transfer coefficients and the effective thermal conductivity of the wick structure (tube and wick). Expressions for calculating the effective thermal conductivity for several widely used wick structures are given by Faghri [0].

4. RESULTS AND DISCUSSION

Results are presented for a fixed air inlet temperature of 40 ^{o}C and inlet air velocities of 1 m/s and 4 m/s under steady state conditions. Four evaporators, each having an effective length of 2.79 metres (external area 0.25m^2), are considered, one for each of the four capillary structures. For simplicity, these are referred to by their characteristic capillary structures, i.e. circular grooves, rectangular grooves, triangular grooves and porous layered. Figure 4 shows boiling heat transfer coefficients for the three grooved tubes. The triangular grooves have higher boiling heat transfer coefficients at a any given groove depth since they have the smallest heat transfer area, as shown in Figure 5, which in turn leads to higher heat fluxes. All of the grooves have an average heat rate of about 220 W at 1 m/s and about 470 W at 4 m/s. This is because the heat transfer conditions outside the bank of tubes remain virtually constant at each air velocity. Hence, the groove depth will have little effect if the heat rate is less than the maximum values shown in Figure 2. At small groove depths, the boiling heat transfer coefficients for the triangular and circular grooves are identical because of the effect of the internal area.

However, the internal area of the circular grooves increases with depth at a higher rate than that for the triangular grooves, approaching and even slightly exceeding that for the rectangular grooves at depths of 0.6 to 0.85 mm. Hence in this region the boiling heat transfer coefficients for the rectangular and circular grooves are identical.In all the cases, the boiling heat transfer coefficient decreases with increasing groove depth because the surface area increases with groove depth as well. Therefore, the heat flux decreases while the driving temperature difference (wall superheated) remains virtually unchanged.

The overall heat transfer coefficient is shown in Figure 6. The trend is similar to that for the boiling heat transfer coefficient with the triangular grooves having marginally larger values of overall heat transfer coefficient. However, the overall heat transfer coefficient appears to be less sensitive to changes in depth than the boiling heat transfer coefficient. This is because the overall heat transfer coefficient includes thermal effects on the air side where the effect of the grooves is minimal. At 1 m/s the values of overall heat transfer coefficient for the triangular grooves and for the circular grooves are similar, while those for the rectangular grooves are lower. The results at 4 m/s follow the same trend as those at 1 m/s. The notable feature is the increased margin by which the overall heat transfer coefficient for the rectangular grooves is lower than that for the circular and triangular grooves. This could be due to the larger volume of liquid contained by the rectangular grooves (Figure 5), which contributes to a lower effective thermal conductivity.

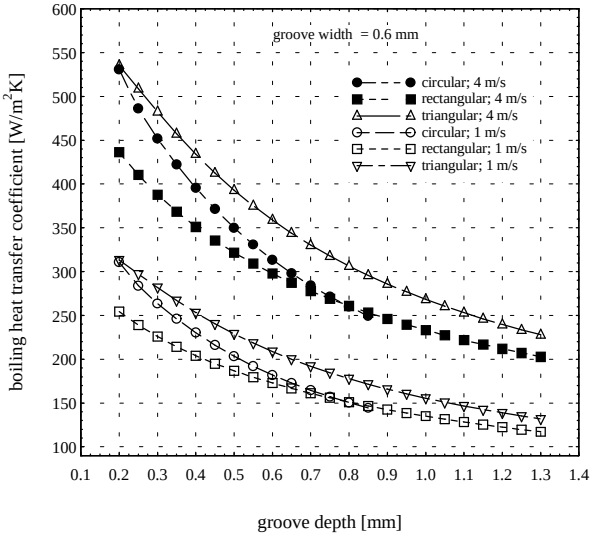

Figure 4: Boiling heat transfer coefficients for the three groove geometries at a fixed groove width of 0.6 mm and varying groove depth.

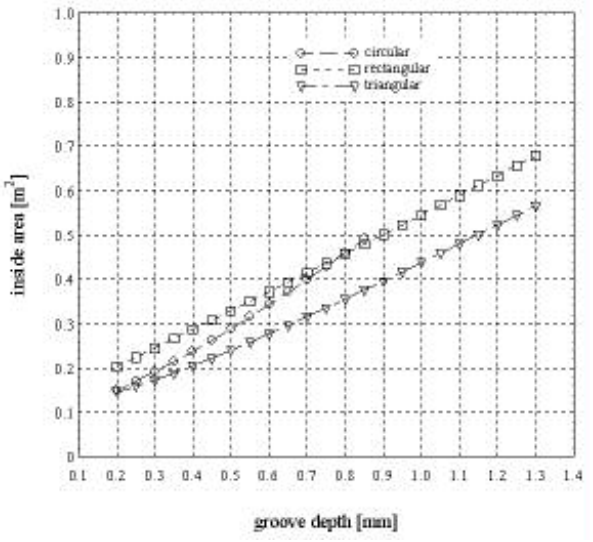

Figure 5: Inside area for the three grooves for a constant groove width of 0.6 mm.

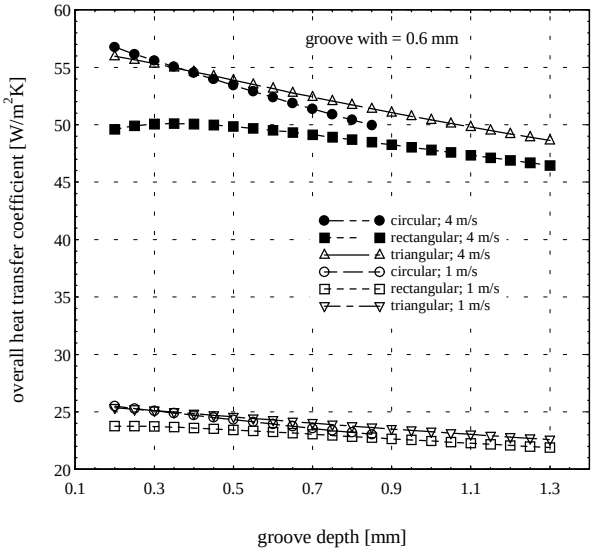

Figure 6: Overall heat transfer coefficients for the three groove geometries at a fixed groove width of 0.6 mm and varying groove depth.

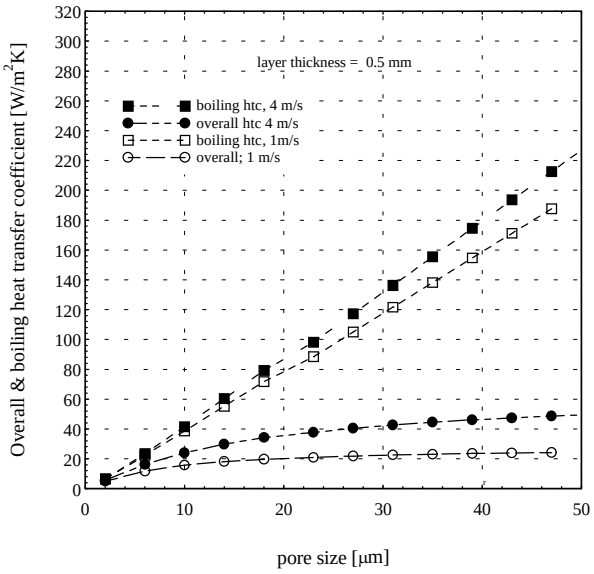

Figure 7: Overall heat transfer coefficient and boiling heat transfer coefficient for tube with a porous inner surface of thickness 0.5 mm and various pore sizes.

Results for the semi-circular grooves are only given up to a groove depth of about 0.8 mm. This is because at depths greater than this value, the capillary head is less than the inner diameter of the evaporator tube and hence the inner circumference of the tube will not be completely wet.

The results for the porous tubes are shown in Figures 7 to 10. The boiling heat transfer coefficient (Figure 7) and heat rate (Figure 8) are seen to be dependant on the pore size to a large extent, both increasing monotonically with pore size. The overall heat transfer coefficients for pore sizes between 20 and 50 μm are comparable to those for the grooves. However, on average the boiling heat transfer coefficients for the porous tubes are seen to be much lower that those for the grooves. In addition, in the case of the porous tubes, the pore size has a significant effect on the heat rate whereas the groove depth had seemingly no effect on the heat rate. The much decreased heat rate at smaller pore sizes can be attributed to reduced permeability. Permeability is a property of the porous material, which characterises its ability to transmit fluid under the action of an applied pressure gradient. Hence, only porous layers characterized by pore sizes greater than 30 μm need to be considered.

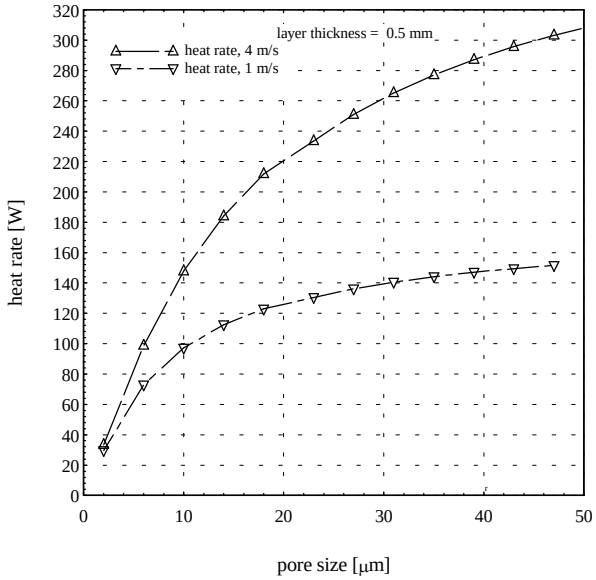

Figure 8: Boiling rate for tube with a porous inner surface of thickness 0.5 mm and various pore sizes.

Figures 9 and 10 show the effect of the thickness of the porous layer on the boiling heat transfer coefficient and overall heat transfer coefficient (Figure 9) and heat rate (Figure 10) for porous layers of particle size 50 μm (20 μm pore size). The overall heat transfer coefficient appears to be insensitive to layer thickness and remains virtually constant over the range. This is because the porous layer has a very small thermal resistance (about 6.5×10^{-4} K/W) compared to the overall thermal resistance, which is about 0.6 K/W. This explanation can be extended to the grooved tubes, where the overall heat transfer coefficient is also insensitive to groove depth (figure 6). The boiling heat transfer coefficient and overall heat transfer coefficient also show marginal variation with layer thickness.

5. CONCLUSIONS

Generally, the heat transfer performance of the three groove geometries is not markedly different from one another. In this work the heat transfer rates are much lower than the maximum rates supported by each

capillary geometry. Hence, it is not surprising that the difference in performance is marginal. However, if the imposed heat flux were to approach the performance limits for the capillary structures, significant differences in heat transfer performance would be apparent. In this light, manufacturing cost would be a significant factor in deciding which capillary structure is best.

The porous tubes show poorer performance in all respects compared to the grooved tubes. This result is heavily dependent on the boiling correlation used for the porous layer and without experimental data, it is difficult to make conclusive remarks.

In this study, the evaporative performance is limited by the outside rate of heat transfer. Hence, considering the fact the evaporator tubes considered are unfinned, the values of heat rate and overall heat transfer coefficients obtained demonstrate the wick structures of the described geometries can be successfully applied in a water evaporator. It is envisaged that a significant improvement in performance could be obtained if the external heat transfer area was increased by the addition of fins.

6. FURTHER WORK

A well-instrumented experimental test rig to complement the analytical work is currently under construction. The experimental results and analytical results will be compared with a view to improving the analytical model.

7. REFERENCES

1 ghri, A., Heat pipe science and technology, Taylor & Francis, Washington, D.C. Taylor & Francis, 1995

2 Eames, I. W., Wu, S. and Sabir, H., "Direct-Heat Exchange Water Evaporator for Vapour Absorption Cycle Refrigerators", IIF-IIR Conference, Norway, 1998.

3 Sabir, H. and Eames, I. W., "Water Film Evaporator for Air-conditioning of Buildings", CIBSE National Conference, 1997.

4 Rohsenow, W. M., "A Method of Correlating Heat Transfer Data for Surface Boiling Liquids", Trans. ASME, Vol. 74, pp. 969, 1952.

5 Stephan, K. and Abdelsalam, M., "Heat-Transfer Correlations for Natural Convection Boiling", Int. J. Heat Mass Transfer, Vol. 23, pp. 73-87, 1980.

6 Cooper, M. G., "Heat Flow Rates in Saturated Nucleate Pool Boiling – a wide-ranging examination using reduced properties", Advances in Heat Transfer, Vol. 16, pp. 325-333, 1984.

7 Incropera, F. P. and De Witt, D. P., *Fundamentals of Heat and Mass Transfer*, 3rd Ed., Wiley, 1990.

8 Madhusudana Rao, S. and Balakrishnan, A. R., "Analysis of Pool Boiling Heat Transfer Over Porous Surfaces", J. Heat and Mass Transfer, Vol. 32, pp. 463-469, 1997.

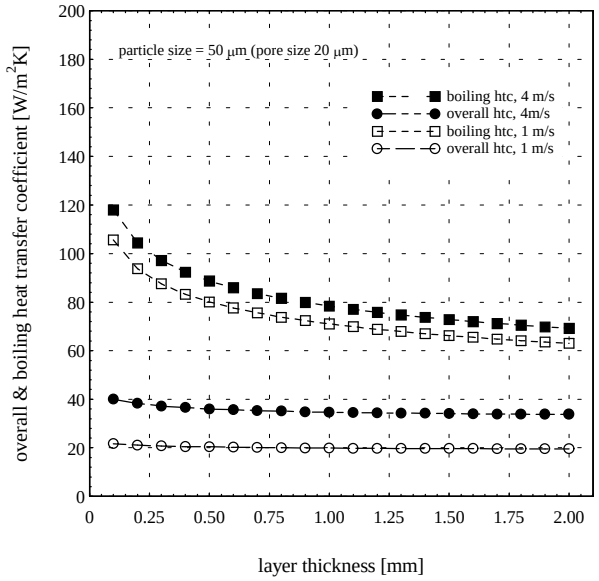

Figure 9: Overall heat transfer coefficient and boiling heat transfer coefficient for tube with a 20 μm (pore size) porous inner surface of various thicknesses.

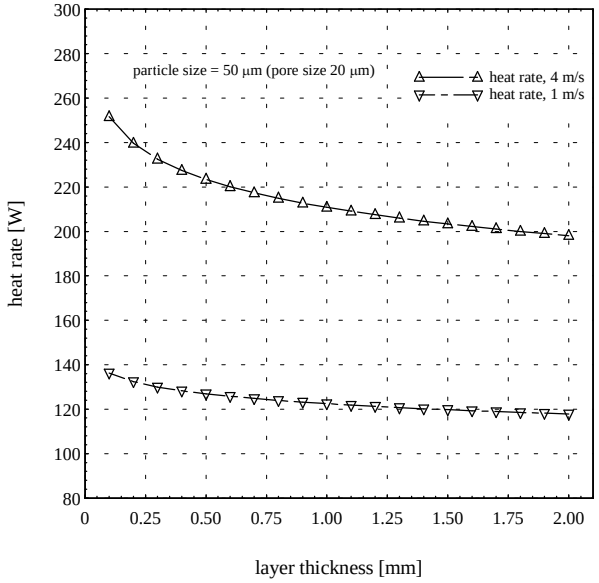

Figure 10: Boiling rate for tube with a 20 μm (pore size) porous inner surface of various thicknesses.

ACKNOWLEDGEMENT:

The authors wish to acknowledge the EPSRC for their support of this work.

NOMENCLATURE

C_p	specific heat capacity	[kg/kJ.K]
C_{sf}	surface coefficient, equation (5)	[-]
d	pore diameter	[m]
d_p	particle diameter for powder	[m]
D_o	evaporator tube O.D	[m]
D_i	evaporator tube I.D	[m]
h	capillary height, equation (2)	[m]

h_{fg}	latent heat of vaporisation [kJ/kg]	
h_{pb}	pool boiling heat transfer coefficient	[W/m^2 K]
G	mass flux	[kg/m^2.s]
k	thermal conductivity	[W/m.K]
K	permeability of porous matrix $= \frac{\varepsilon d^2}{32}$	[m^2]
q	heat rate	[W]
q''	heat flux	[W/m^2]
r_c	capillary radius	[m]
r_e	effective radius	[m]
r_h	hydraulic radius	[m]
S_{TL}	ratio of traverse to lateral pitch Equation (4)	[-]
T	temperature	[K]

Greek Letters

δ	thickness of porous layer	[m]
ΔT	temperature difference	[K]
ε	porosity	[-]
μ	viscosity	[N.s/m^2]
θ	contact angle	[rad]
ρ	density	[kg/m^3]
σ	surface tension	[N/m^2]

Subscripts

g	vapour
l	liquid
max	maximum value
sat	saturation condition
w	tube wall

Abbreviations

max	maximum
O.D	outer diameter
I.D	inner diameter
Sat	saturation

Dimensionless Groups

Ja	Jacob number = $\frac{\rho_l Cp_l \Delta T}{\rho_g h_{fg}}$
Nu	Nusselt number = $\frac{hr_h}{k}$
Pr	Prandtl number = $\frac{C_p \mu}{k}$
Re	Reynolds number = $\frac{GD_o}{\mu}$